


Cite this: *RSC Adv.*, 2023, 13, 26545

# Metal-enhanced fluorescence through conventional Ag-polyethylene glycol nanoparticles for cellular imaging

Chih-Jung Chen,<sup>abc</sup> Chun-Yen Wu,<sup>d</sup> Chi-Wei Wu,<sup>d</sup> Ching-Wen Chang,<sup>d</sup> Tsung-Tao Huang,<sup>e</sup> Ming-Hua Shiao,<sup>e</sup> Chu-Kuei Lin,<sup>f</sup> Yu-Chun Chen<sup>\*d</sup> and Yung-Sheng Lin<sup>id</sup> <sup>\*d</sup>

A novel application of conventional Ag nanoparticles (NPs) for metal-enhanced fluorescence (MEF) in cellular imaging is proposed. Different molecular weights of polyethylene glycol (PEG) were tested to determine a suitable spacer on Ag NPs for MEF, and NPs comprising Ag with PEG with a molecular weight of 6000 g (Ag-PEG6k), when present in fluorescein solution, were discovered to cause a 2-fold quantum yield enhancement. For fluorescence imaging of mesenchymal stem cells stained by Alexa Fluor 488, the enhancement factor increased with the Ag-PEG6k NP concentration but decreased with the Alexa Fluor 488 concentration. At 243 parts per billion Ag-PEG6k NPs and 625 parts per million Alexa Fluor 488, the enhancement factor reached its greatest value of over 4.

Received 6th April 2023  
Accepted 21st August 2023

DOI: 10.1039/d3ra02277c

rsc.li/rsc-advances

## Introduction

There is an increasing demand for image analysis for biological sciences and clinical applications.<sup>1</sup> Advances in imaging have allowed researchers to access more information in the biosciences and biomarkers for disease identification, progress, and treatment responses.<sup>2</sup> Progress in optics enables imaging from single molecules to entire organisms. However, conventional and cheap materials are important for applications of optical technology. Costly materials are an issue for applications.

Fluorescence technology is currently used in many areas—such as chemical analysis, biomedical imaging, and clinical analysis—due to its fast response, sensitivity, reproducibility, and multiple optical parameters.<sup>3</sup> However, in many biological and medical applications, trace amounts of biomolecules must be detected, and many biomolecular signals obtained through ordinary observation are weak. Therefore, the fluorescence signals of detection targets must be improved for observation.

Metal nanomaterials have resulted in new developments in fluorescence technology. Metal surfaces or nanostructures can interact with fluorophores to enhance their fluorescence

intensity.<sup>3</sup> Metal nanostructures and metal colloidal nanoparticles (NPs) are effective for increasing fluorophores' fluorescence because they can interact with proximal fluorophores at optimal distances of 5–90 nm to increase the quantum yield; this phenomenon is known as surface-enhanced fluorescence or metal-enhanced fluorescence (MEF).<sup>4,5</sup> Under photon excitation, noble-metal NPs generate plasma to amplify the excitation of fluorophores close to their surface, enhancing the fluorescence.<sup>6</sup>

Gontero *et al.* deposited Au@SiO<sub>2</sub>–rhodamine B NPs on *Escherichia coli* bacteria for bioimaging over their surface and reported an optimal enhancement factor of 9.5 for 10 nm silica spacers.<sup>7</sup> Dong *et al.* used anti-human CD71 antibodies to label the transferrin receptors of Ramos cells and investigated the MEF of rhodamine B by using core-shell Au@SiO<sub>2</sub>–rhodamine B NPs. The mean fluorescence intensities of cells labeled by control NPs lacking Ag core and core-shell NPs were 5000 and 8700, respectively.<sup>8</sup> Zhai *et al.* (2020) studied Au-nanofilm-enhanced fluorescence on HeLa cells stained using 1,1'-diocetadecyl-3,3,3',3'-tetramethylindocarbocyanine perchlorate (for membranes), propidium iodide (for dsDNA in nuclei), and acridine orange (for dsDNA, ssDNA, and RNA in both the nucleus and cytoplasm). The fluorescence enhancement decreased as the distance from the Au nanofilm surface was increased; the largest enhancement factor was 5.9.<sup>3</sup>

In the literature, the MEF material applied for labeling microorganisms or cells is typically based on Au NPs. However, few studies have investigated cheap and conventional Ag NPs for MEF applications. This study developed Ag NPs, which can be fabricated through a simple and inexpensive process, to be used in effective MEF-based cellular imaging.

<sup>a</sup>Department of Pathology and Laboratory Medicine, Taichung Veterans General Hospital, Taichung 407219, Taiwan

<sup>b</sup>School of Medicine, Chung Shan Medical University, Taichung 402306, Taiwan

<sup>c</sup>Department of Post-Baccalaureate Medicine, College of Medicine, National Chung Hsing University, Taichung 402202, Taiwan

<sup>d</sup>Department of Chemical Engineering, National United University, Miaoli 360302, Taiwan. E-mail: joycechen@nuu.edu.tw; liny@nuu.edu.tw

<sup>e</sup>Taiwan Instrument Research Institute, National Applied Research Laboratories, Hsinchu 302058, Taiwan

<sup>f</sup>PoloWang Bio. Inc, New Taipei City 234011, Taiwan


## Experimental section

### Preparation of Ag-PEG NPs

Polyethylene glycol (PEG, Ferak, Berlin, Germany) with three molecular weights—4000, 6000, and 20 000 Da, abbreviated as PEG4k, PEG6k, and PEG20k, respectively—was used as a spacer on the Ag NPs for MEF. Ag-PEG NPs were synthesized using a sodium citrate reduction method and PEG adsorption. In brief, 2 mL of 1 mM freshly prepared silver nitrate (99.995%, Echo Chemical, Miaoli, Taiwan) solution was added to 10 mL of 20 mM sodium citrate (99%, Sheng-I Chemical, Taichung, Taiwan) solution. The mixture containing PEG was stirred for 30 minutes at room temperature, and Ag-PEG NPs were obtained. The zeta potential (Zetasizer Pro, Malvern Panalytical, UK), UV-vis (U-2900, HITACHI, Japan), and infrared spectroscopy (Nicolet iS10, Thermo Scientific, USA) were performed to characterize the system in the absence and presence of PEG.

### Transmission electron microscopy analysis

The size and shape of the Ag-PEG6k NPs were determined using transmission electron microscopy (TEM; JEM-2010, JEOL, Japan) with an accelerating voltage of 200 kV. A drop of Ag-PEG6k NP solution was placed on the TEM grid (carbon-copper grid) until its complete adsorption. Excess Ag-PEG6k NP solution on the TEM grid was removed before the subsequent analysis.

### Cellular imaging

To confirm the MEF effect of the Ag-PEG6k NPs, Alexa Fluor 488 anti- $\beta$ -actin antibody (BioLegend, CA, USA) was used to stain human mesenchymal stem cells (MSCs; SCC034, Merck, Germany). Cells were seeded on an ibidi  $\mu$ -Slide 8 Well at a density of  $1 \times 10^4$  cells per well. After 1 day of cultivation, the cells were fixed with 3.7% formalin (Thermo Fisher Scientific, Waltham, MA, USA) overnight and permeabilized with 0.5% Triton X-100 (Sigma-Aldrich, St. Louis, MO, USA) for 30 minutes. After several PBS washes, the cells were blocked with 5% FBS (Thermo Fisher Scientific, Waltham, MA, USA) for 30 minutes and stained by 0, 625, 1250, or 2500 parts per million (ppm) dye with or without 0, 24.3, 48.6, 121.5 or 243 parts per billion (ppb) Ag-PEG6k NPs in a blocking buffer overnight at 4 °C in the dark. Alexa Fluor 488 anti- $\beta$ -actin with a dye concentration of 0, 625, 1250, and 2500 ppm was used for the 0, 0.625, 1.25, and 2.5  $\mu\text{L mL}^{-1}$  solutions, respectively. Images were obtained using a fluorescence microscope (ECLIPSE, Nikon, Japan), and the quantitative fluorescence intensity was analyzed using ImageJ.

### Cytotoxicity

Cytotoxicity of Ag-PEG6k NPs was evaluated by WST-8 assay (BioVision, USA). MSCs were seeded in 96-well plates with a density of  $6 \times 10^3$  cells per well. Ag-PEG6k NPs with various concentrations were added into each well for cytotoxicity evaluation. After 1- and 3 days cultivation, cells were reacted with 1-methoxy-5-methylphenazinium methyl sulfate in WST-8 assay, and the absorbance at 450 nm was measured.

## Results and discussion

Fig. 1–3 are zeta potential, UV-vis, and infrared spectrum, respectively, of the system in the absence and presence of PEG. The zeta potential (Fig. 1) of Ag-PEG6k NPs is  $-35$  mV, revealing good colloidal stability of Ag-PEG6k NPs in the solution.<sup>9</sup> However, Ag NPs, Ag-PEG4k NPs, and Ag-PEG20k NPs have poor colloidal stability due to low zeta potentials. The UV-vis spectrum (Fig. 2) of Ag NPs exhibits the absorbance peak between 350 nm and 450 nm,<sup>9,10</sup> and shows smaller absorbance than Ag-PEG NPs. The Ag-PEG6k NPs have higher absorbance than Ag-PEG4k and Ag-PEG20k NPs. The infrared spectrum (Fig. 3) of Ag NPs and Ag-PEG NPs are similar. However, the small peak has a slight shift from  $1639.68\text{ cm}^{-1}$  (Ag NPs) to  $1640.16\text{ cm}^{-1}$  (Ag-PEG NPs), indicating the hydrogen bonding between PEG and water.

Fig. 4(a) presents the fluorescence spectrum of  $5 \times 10^{-5}$  wt% fluorescein solutions containing the various Ag-PEG NPs (243 ppb). The results indicate that the maximum fluorescence wavelength has a red-shift of 3 nm for all three Ag-PEG NP solutions, indicating the interaction of fluorescein with Ag-PEG NPs. This result agrees with the results of the experiment of Liu *et al.* They used Ag-SiO<sub>2</sub> NPs in the solution and found a red-shift of 10 nm in the maximum wavelength.<sup>11</sup> Regarding the fluorescence intensity, the Ag-PEG NPs significantly increase the intensity in the fluorescence spectrum of the fluorescein solution, regardless of the PEG molecular weights. Fig. 4(b) presents a quantum yield comparison of the base fluorescein solution and the solutions with the three types of Ag-PEG NPs. Agreeing with the previous report,<sup>12</sup> the base fluorescein solution has a quantum yield of 0.33. Ag-PEG6k NPs result in the maximum quantum yield of 0.65. The fluorescence enhancement factor of the Ag-PEG6k NPs is approximately 2, and this value corresponds to the result for AgNPs-PNIPAM reported by Tang *et al.* (2011).<sup>13</sup> The molecular length of PEG4k, PEG6k, and PEG20k is approximately 1.9 nm,<sup>14</sup> 3.97 nm,<sup>15</sup> and 20.5 nm,<sup>16</sup> respectively. Therefore, the best thickness of PEG on Ag NPs for MEF is approximately 4 nm, and the Ag-PEG6k NPs were used for further cell experiments in this study.

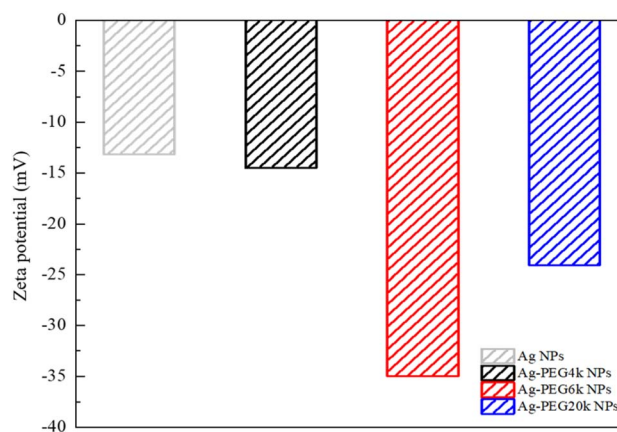


Fig. 1 Zeta potential of Ag NPs and different Ag-PEG NPs.



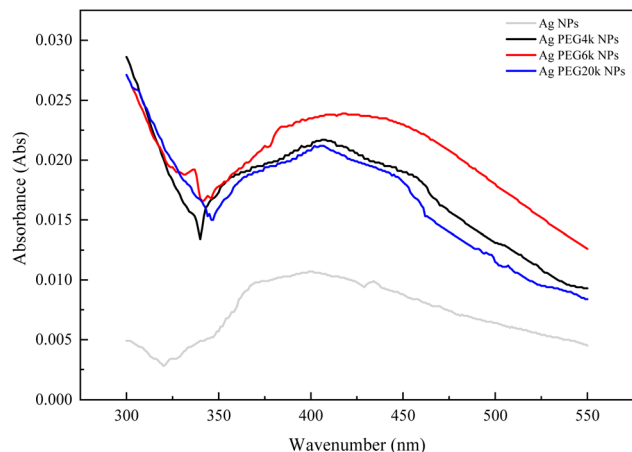


Fig. 2 UV-vis spectrum of Ag NPs and different Ag-PEG NPs.

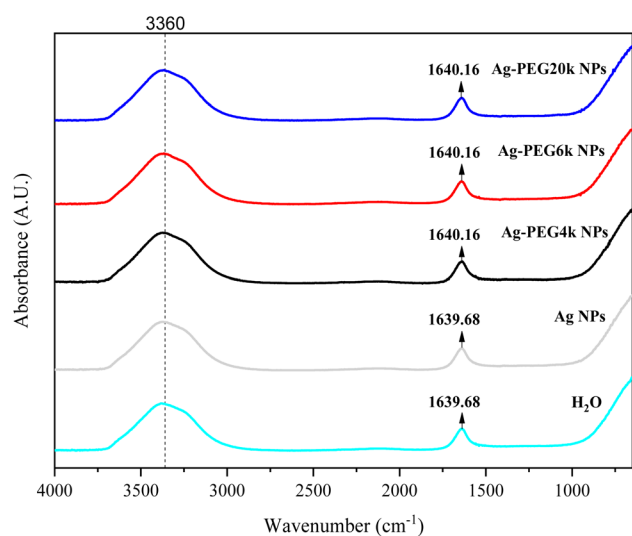


Fig. 3 Infrared spectrum of Ag NPs and different Ag-PEG NPs.

Fig. 5(a) presents a TEM bright field image of the prepared Ag-PEG6k NPs with a 243 ppb concentration in solution, as was determined through inductively coupled plasma analysis. The morphology of the Ag-PEG6k NPs is irregular and not spherical. The particle size distribution of the Ag-PEG6k NPs is shown in Fig. 5(b) for 300 particles in the TEM pictures; the average particle size is  $4.78 \pm 1.35$  nm.

Fig. 6 presents pictures of MSCs stained with Alexa Fluor 488 by optical, fluorescence, and merged images, indicating cells with green fluorescence. The results of various gradient concentrations of Alexa Fluor 488 dye and Ag-PEG6k NPs are compared in Fig. 7. The maximum concentration of Alexa Fluor 488 dye was 2500 ppm. After equal volume serial dilution, the dye at 625, 1250, and 2500 ppm concentrations were used for cell staining. Besides, we also used a staining solution with 0 ppm dye concentration for nanoparticle autofluorescence confirmation. The first column of Fig. 7 displays images corresponding to Ag-PEG6k NP treatment but no Alexa Fluor 488 dye

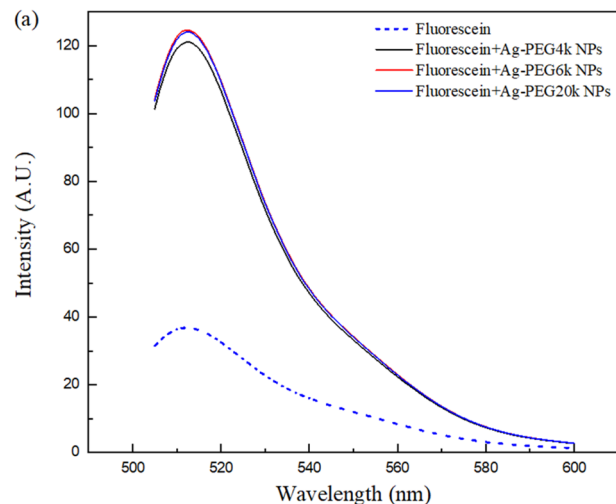


Fig. 4 (a) Fluorescence spectrum and (b) quantum yield of fluorescein solutions containing different Ag-PEG NPs.

staining; the results are black images without any fluorescence. After staining the  $\beta$ -actin of MSCs with Alexa Fluor 488 dye, cellular fluorescence signals can be observed (first row of Fig. 7). Some faint green cell images are visible for the MSCs stained with only 1250 or 2500 ppm Alexa Fluor 488 dye. To confirm the fluorescence enhancement ability of NPs, we prepared gradient concentrations of NPs from 24.3 to 243 ppb. Results show that

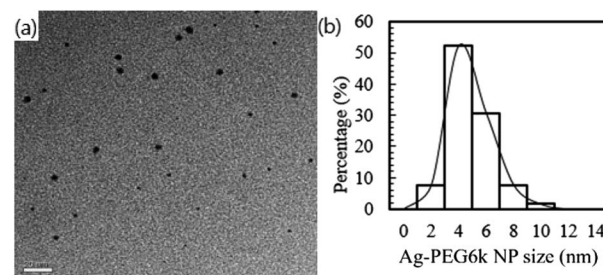


Fig. 5 (a) TEM image showing the morphology of the Ag-PEG6k NPs, which were synthesized using the sodium citrate reduction method and PEG adsorption. The scale bar is 20 nm. (b) Particle size distribution of the Ag-PEG6k NPs in the TEM image.





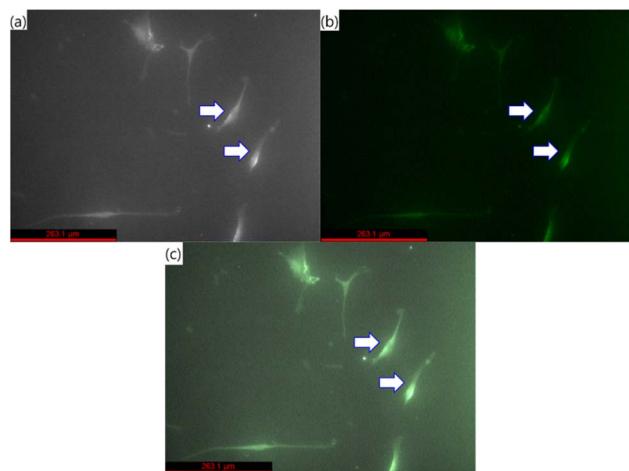


Fig. 6 (a) Optical, (b) fluorescence, and (c) merged images of MSCs stained with Alexa Fluor 488. Arrows indicated cells, and the scale bar is 263.1  $\mu\text{m}$ .

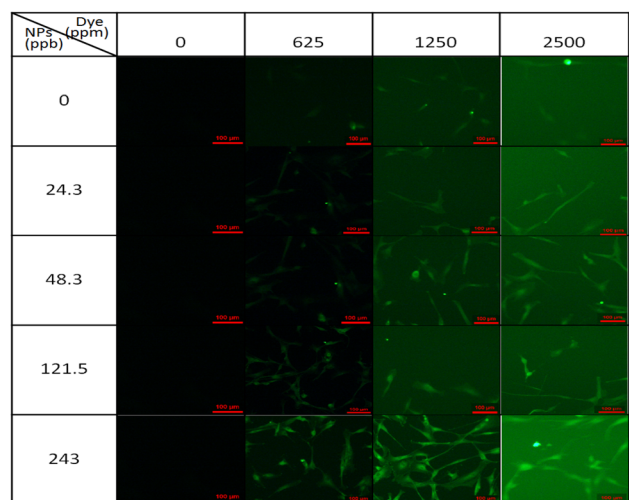


Fig. 7 Fluorescence images of  $\beta$ -actin distribution in MSCs stained by Alexa Fluor 488 and Ag-PEG6k NPs. (Scale bar is 100  $\mu\text{m}$ ).

increasing the concentration of the Ag-PEG6k NPs boosted the cellular fluorescence signal. Clear images of green fluorescent cells were obtained for the Ag-PEG6k NP groups; those for the high-concentration (243 ppb) group were particularly clear.

Fig. 8(a) presents the results of a quantitative analysis of the cell images displayed in Fig. 7 to determine the effect of Alexa Fluor 488 concentration on cellular fluorescence for various Ag-PEG6k NP concentrations. One hundred cells were counted to ensure adequate statistical representation for the imaging studies. A higher concentration of Alexa Fluor 488 resulted in greater fluorescence intensity. The low fluorescence intensity without Alexa Fluor 488 is the background signal of the observation image system. Fig. 8(b) reveals the enhancement factor of the various Ag-PEG6k NP concentrations by normalizing the fluorescence intensity for each Alexa Fluor concentration to that of the corresponding intensity without the Ag-PEG6k NPs in

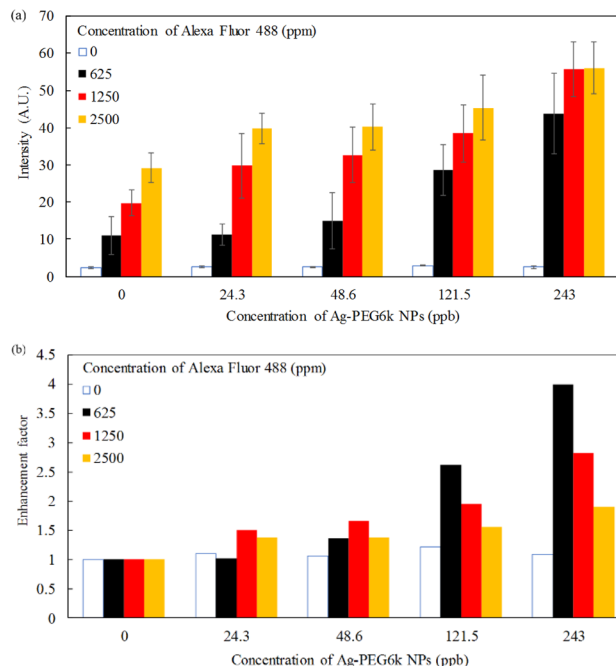


Fig. 8 (a) Fluorescence intensity and (b) enhancement factor of various Ag-PEG6k NP concentrations for  $\beta$ -actin in MSCs stained by Alexa Fluor 488.

Fig. 8(a). The enhancement factor increases as the Ag-PEG6k NP concentration increases. However, this concentration has a weak effect on the enhancement factor if the Ag-PEG6k NP concentration is small (24.3 and 48.6 ppb). The enhancement factor also decreases with the Alexa Fluor 488 concentration for the high-concentration Ag-PEG6k NPs (121.5 and 243 ppb). At 243 ppb Ag-PEG6k NPs and 625 ppm Alexa Fluor 488, the enhancement factor reaches its largest value of greater than 4.

Fig. 9 shows cell images of MSCs treated with different concentrations (0 ppb, 0.0243 ppb, 0.243 ppb, 2.43 ppb, 24.3 ppb, and 243 ppb) of Ag-PEG6k NPs. It can be found that there are nearly no cells in the high Ag-PEG6k NP concentration group, 243 ppb Ag-PEG6k NPs group (Fig. 9(f)). Besides, there is no significant difference in cell images among the control (0 ppb Ag-PEG6k NPs) and low concentration groups (0.0243

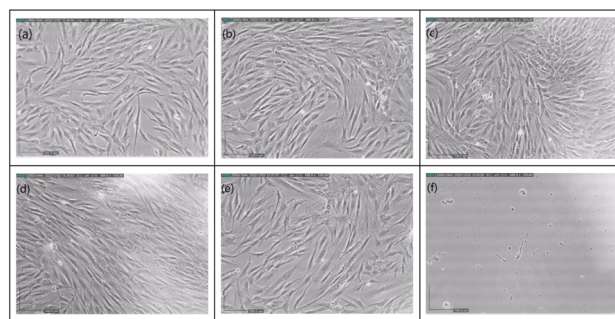


Fig. 9 Cell images of MSC treated with different concentrations of Ag-PEG6k NPs (a) 0 ppb; (b) 0.0243 ppb; (c) 0.243 ppb; (d) 2.43 ppb; (e) 24.3 ppb; (f) 243 ppb.



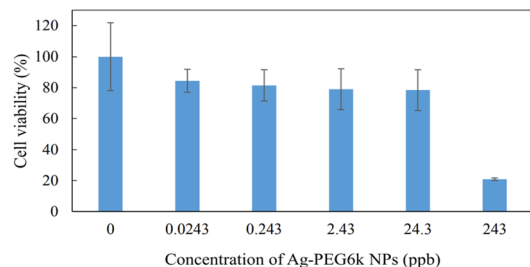


Fig. 10 The cell viability in different concentrations of Ag-PEG6k NPs. ( $n = 6$ ,  $n$  means experiment repeat times).

ppb, 0.243 ppb, 2.43 ppb, and 24.3 ppb Ag-PEG6k NPs). In order to quantitative the cell viability of nanoparticles treated MSCs and observe the influence of Ag-PEG6k NPs on cells, WST assay was applied to examine the mitochondrial activity of the cells. Fig. 10 shows the results of MSCs treated with different concentrations of Ag-PEG6k NPs. The cell viability decreased significantly in the 243 ppb Ag-PEG6k NPs group compared with that in the control group. The cell viability was only 20% in the 243 ppb Ag-PEG6k NPs group. However, the cell viability was about 80 to 90% in other groups (0.0243 ppb, 0.243 ppb, 2.43 ppb, and 24.3 ppb Ag-PEG6k NPs groups). These results show that the Ag NPs functionalized with PEG6k under the concentration below 24.3 ppb have acceptable cell viability. However, a high Ag-PEG6k NP concentration, such as 243 ppb, can be used for applications to increase the fluorescent staining intensity of dead and fixed cells. Several basic and important staining techniques, such as phalloidin for cytoskeleton actin filament staining, DAPI for nuclear counterstain, and annexin V staining for apoptosis detection, use fixed cells for fluorescent staining. Besides, lots of clusters of differentiation (CD) markers staining also use paraformaldehyde-fixed cells for cell identification. The Ag-PEG6k NPs developed are expected to be used in the above experiments to enhance the fluorescent signal and accurately distinguish the differences between groups.

## Conclusions

This study developed conventional Ag NPs as a MEF material to enhance cellular imaging. PEG with different molecular weights was selected as spacer on the Ag NPs. Ag-PEG6k NPs had the maximum quantum yield. The fluorescence enhancement factor for staining  $\beta$ -actin in human MSCs increased with the Ag-PEG6k NP concentration but decreased with the Alexa Fluor 488 concentration. The optimal MEF was obtained at 243 ppb Ag-PEG6k NPs and 625 ppm Alexa Fluor 488; the enhancement factor was greater than 4. Therefore, Ag-PEG6k NPs are a feasible MEF material for cellular imaging.

## Author contributions

Conceptualization: Chih-Jung Chen, Yu-Chun Chen, and Yung-Sheng Lin; investigation: Chih-Jung Chen, Yu-Chun Chen, and

Yung-Sheng Lin; data curation: Chun-Yen Wu, Chi-Wei Wu, Ching-Wen Chang, Chu-Kuei Lin, Tsung-Tao Huang, and Ming-Hua Shiao; funding acquisition and supervision: Chih-Jung Chen, Yu-Chun Chen, and Yung-Sheng Lin; writing – original draft: Chih-Jung Chen, Yu-Chun Chen, and Yung-Sheng Lin; writing – review and editing: Yung-Sheng Lin. All authors have read and agreed to the published version of the manuscript.

## Conflicts of interest

There are no conflicts to declare.

## Acknowledgements

The following funding is acknowledged: Taichung Veterans General Hospital/National United University Joint Research Program (TCVGH-NUU1118905) and National Science and Technology Council, Taiwan (111-2314-B-239-002).

## Notes and references

- 1 M. Wang, C.-C. Mi, W.-X. Wang, C.-H. Liu, Y.-F. Wu, Z.-R. Xu, C.-B. Mao and S.-K. Xu, *ACS Nano*, 2009, **3**(6), 1580–1586.
- 2 D. Udhayakumari and V. Inbaraj, *J. Fluoresc.*, 2020, **30**, 1203–1223.
- 3 Y.-Y. Zhai, Q. Liu, W.-P. Cai, S.-H. Cao, L.-X. Zhang and Y.-Q. Li, *J. Phys. Chem.*, 2020, **124**, 2760–2768.
- 4 Y. Jeong, Y.-M. Kook, K. Lee and W.-G. Koh, *Biosens. Bioelectron.*, 2018, **111**, 102–116.
- 5 R. Bukasov, Z. Kunushpayeva, A. Rapikov, S. Zhunussova, A. Sultangazyev and O. Filchakova, *J. Fluoresc.*, 2020, **30**, 1477–1482.
- 6 H. Zhang, M.-H. Cao, W. Wu, H. Xu, S. Cheng and L.-J. Fan, *Nanoscale*, 2015, **4**, 1–3.
- 7 D. Gontero, A.-V. Veglia, D. Boudreau and A.-G. Bracamonte, *J. Nanophotonics*, 2018, **12**(1), 012505.
- 8 M. Dong, Y. Tian and D. Pappas, *Anal. Methods*, 2014, **6**, 1598–1602.
- 9 K. Shameli, M.-B. Ahmad, S.-D. Jazayeri, S. Sedaghat, P. Shabanzadeh, H. Jahangirian, M. Mahdavi and Y. Abdollahi, *Int. J. Mol. Sci.*, 2012, **13**, 6639–6650.
- 10 K. S. V. K. Rao, P.-R. Reddy, Y.-I. Lee and C. Kim, *Carbohydr. Polym.*, 2012, **87**, 920–925.
- 11 X. Liu, D. Li, X. Sun, Z. Li, H. Song, H. Jiang and Y. Chen, *Sci. Rep.*, 2015, **5**, 12555.
- 12 R. Boonsin, G. Chadeyron, J.-P. Roblin, D. Boyerab and R. Mahiou, *J. Mater. Chem. C*, 2016, **4**, 6562–6569.
- 13 F. Tang, N. Ma, X. Wang, F. He and L. Li, *J. Mater. Chem.*, 2011, **21**, 16943.
- 14 G. Manon, B. Emilie and S. R. Cécile, *Colloids Surf., B*, 2014, **123**, 770–777.
- 15 S. Liufu, H. Xiao and Y. Li, *Powder Technol.*, 2004, **145**, 20–24.
- 16 W. Wang, Q.-Q. Wei, J. Wang, B.-C. Wang, S.-H. Zhang and Z. Yuan, *J. Colloid Interface Sci.*, 2013, **404**, 223–229.

